Journal of Applied Polymer Science

Self-Welding 1-Butene/Ethylene Copolymers from Metallocene Catalysts: Structure, Morphology, and Mechanical Properties

Carla Marega,[1] Stefano Spataro,[2] Elisa Fassone,[2] Isabella Camurati,[2] Antonio Marigo[1]
[1]Dipartimento di Scienze Chimiche, Università di Padova, via Marzolo 1 Padova I-35131, Italy
[2]Basell Poliolefine Italia Srl Centro Ricerche G.Natta, Ferrara I-44100, Italy
Correspondence to: C. Marega (E-mail: carla.marega@unipd.it).

ABSTRACT: Samples of random copolymers consisting of 1-butene modified with a low ethylene content (4, 5, 8% by weight) produced with metallocene catalysts were studied to elucidate the polymorphic behavior of this new class of materials and to characterize them from a structural, morphological, and mechanical point of view. The samples cooled down from the melt are in amorphous phase and crystallize in a mixture of form I and I′ or in pure form I′ with aging time, according to the C2 content. Infrared and nuclear magnetic resonance spectroscopy, X-ray diffraction and microscopic techniques were used to follow the changes of the material with aging time and to correlate the structural and morphological behavior with the peculiar mechanical properties that differentiate the samples with increasing C2 content. The presence, in the aged samples with higher C2 content, of the pure form I′ induces the peculiar ability to self-welding and these copolymers combine high flexibility with good elasticity and ductility and can be processed directly or used as modifying agents in polymers. © 2013 Wiley Periodicals, Inc. J. Appl. Polym. Sci. **2014**, *131*, 40119.

KEYWORDS: copolymers; spectroscopy; X-ray; microscopy; mechanical properties

Received 10 July 2013; accepted 24 October 2013
DOI: 10.1002/app.40119

INTRODUCTION

Isotactic poly-1-butene (IPB) was first synthesized, by Natta et al.,[1] in 1954. It exhibits advantages over the other polyolefins in toughness, tear strength, flexibility, creep, stress cracking resistance, impact resistance, abrasion resistance, and high temperature resistance.

However IPB is still produced in limited quantities and has not yet found a large commercial success if compared with the other polyolefins, this can be attributed to the peculiar crystallization behavior of the polymer.

IPB can exist in several polymorphous crystalline forms I, II, I′, III, depending on the way it is produced. IPB generally crystallizes from the melt prevalently in form II, tetragonal[2] but, upon cooling, it spontaneously transforms into the thermodynamically stable form I, hexagonal.[3–5] This transformation takes about one week under normal conditions and is reflected in important changes in the physical-mechanical properties. During the form transformation II → I, density, cristallinity, hardness, rigidity, stiffness, and tensile strength increase to values characteristic of form I. The relatively constant values for ultimate tensile strength and elongation indicate that stretching or orientation accelerate the form transformation II → I.

This transition also involves a change in the chain conformation: the 11_3 helix of form II converts into a 3_1 helix of the modification I. Such a structural change requires an elongation of helical axis.

The study of this transition was carried out by different experimental techniques such as wide angle X-ray diffraction (WAXD),[3–9] differential scanning calorimetry (DSC),[9–11] small angle X-ray scattering (SAXS).[12]

Form III, orthorhombic[13–16] and form I′, hexagonal[4,14,17] are generally obtained by crystallization from dilute solutions depending on the solvent used, the concentration and temperature of crystallization.

WAXD studies of single crystal show that form I and form I ' have the same hexagonal cell, but form I is a "twinned" form while I′ is "untwinned"[2]. Other differences between the two modifications are the melting temperature and the infrared spectra.[17] For these reasons, form I′ is often defined as an imperfect form I.[18]

One of the approaches proposed for increasing the rate of form transformation II → I is to use copolymers of 1-butene. When ethylene (C2) comonomeric units are inserted in the IPB chains,

Additional Supporting Information may be found in the online version of this article.

Table I. Samples Characterization

		PBET4	PBET5	PBET8	PBET8-A1	PBET8-A2
C2	wt %	4.1	5	8	8	8.2
TerPP	wt %	0	0	0	8.9	15.4
$\overline{M}_w/\overline{M}_n$		2.1	2.2	2.5	2.5	2.4
$\overline{M}_w$		420700	358900	274500	383500	454200
Density	Kg/dm^3	0.8863	0.8841	0.8680	0.8727	0.8708
C_{WAXD}	%	31	24	8	8	7
Tm_r	°C	38.8	38.3	39.6	38	37.9
Tm_I	°C	54.6	51.7			

crystallization from the melt produces the appearance of two populations of form II, differing by structural order and by the amount of constitutional defects incorporated.[19,20]

The more defective population exhibits a much faster II→I conversion rate than the ordered ones, thus leading to the formation of form I at very short aging time.[19]

Even more effective was proved to be the preparation of nanocomposites based on a copolymer of 1-butene and ethylene filled with montmorillonite, from which the crystallization from the melt was directly obtained in form I.[21]

Most of the studies have been focused on samples prepared with Ziegler-Natta catalysts, but it has been proved of great interest the study of IPB samples produced with metallocene catalysis, for which it has been observed that the most stereodefective samples crystallize from the melt as mixtures of form II and form I or directly in form I depending on the percentage of defects and the cooling rate.[22]

In this article, we report a structural and morphological study of samples of random copolymers consisting of 1-butene modified with a low ethylene content (4, 5, 8% by weight) produced with metallocene catalysts. The ethylene content in the copolymer of 1-butene influences the physical properties of the final product, in fact increasing the content of ethylene decrease the crystallization rate, the melting temperature and the crystallinity.

The crystalline form obtained from the melt depends on the experimental conditions (pressure, cooling rate etc.), the molecular weight of the samples and the ethylene content. 1-butene copolymers with an ethylene content of less than 3% by weight crystallize from the melt in form I and form II, the fraction of form I increases with the ethylene content.

The rate of the transition (solid–solid) from form II to form I is higher in the presence of ethylene, on an equal molecular weight.[19]

In the samples produced by metallocene catalysis, the decrease of crystallinity and the melting temperature is faster compared with copolymers synthesized by Ziegler-Natta catalysts.

Another peculiarity of these samples is that, when the ethylene content is higher than 3–4% by weight, they do not crystallize from the melt. The samples are in the amorphous state just cooled down to room temperature. In the samples subjected to aging it is possible to observe the crystallization directly in form I (or I′), so there is no solid–solid transformation from form II to form I.

The structure of these materials has been studied by X-Ray diffraction (WAXD), nuclear magnetic resonance in the solid state (SS NMR), infrared spectroscopy (IR and ATR) and DSC. The morphological study was carried out by SAXS, transmission electron microscopy (TEM) and atomic force microscopy (AFM).

The information obtained was correlated to the final properties of this new class of materials which combine high flexibility with good elasticity and very high ductility, so that they can be processed directly or used as modifying agents in polymers.

EXPERIMENTAL

Samples of random copolymers consisting of 1-butene modified with a low ethylene content were prepared in the laboratories of Lyondellbasell Polyolefins (Ferrara, Italy) with metallocene catalysts.[23–25]

The polymerization was carried out in liquid monomer of 1-butene at 70°C in a single continuous reactor to produce copolymers with a weight percentage of ethylene between 0 and 20%.

The samples differ in the percentage of ethylene content (4, 5, 8% by weight) and two samples (PBET8-A1 and PBET8-A2) were mixed with a terpolymer based on polypropylene, called terpolymer (terPP), compatible with IPB both chemically and thermally, whose purpose is to act as a nucleating agent to obtain pellets from the copolymers with a high ethylene content, since it accelerates the crystallization rate.

All the samples were prepared from pilot plant except PBET8-A1 which was produced from industrial plant.

The characteristics of the samples studied are reported in Table I.

Infrared and Attenuated Total Reflectance Spectroscopy

FTIR measurements were performed in a Nicolet spectrophotometer Magna-IR 760, operating in transmission in the range 400–4000 cm^{-1}, with a resolution of 2 cm^{-1} and collecting 64 scans.

Films of about 0.2-mm thickness were prepared by compression molding of the samples, FTIR spectra were recorded at different aging times.

ATR spectra were carried out on powder samples with a Nicolet spectrophotometer Magna System 560, operating in the range 650–5000 cm^{-1}, with a resolution of 4 cm^{-1} and collecting 128 scans.

Differential Scanning Calorimetry

All the measurements were carried out with a Perkin-Elmer Pyris 1 DSC calorimeter operating under N_2 atmosphere. Polymer samples weighing about 5 mg closed in aluminum pans were used throughout the experiments. Indium of high purity was used for calibrating the DSC temperature and enthalpy scales.

Samples were first heated from 20°C to 180°C at 10°C/min and kept in isotherm at that temperature for 5 min, then cooled down from 180°C to −20°C, kept at −20°C for 5 min, followed by a second heating ramp from −20°C to 180°C, kept at 180°C for 5 min, then cooled down from 180°C to 20°C (always at 10°C/min).

The capsule of the DSC samples was then kept at room temperature and atmospheric pressure for the aging time chosen, after which the measurements were done on the aged samples heating from 20°C to 180°C.

Wide Angle X-ray Diffraction

WAXD patterns were recorded in the diffraction angular range 5–25° 2θ by a Philips X'Pert PRO diffractometer, working in the reflection geometry and equipped with a graphite monochromator on the diffracted beam, CuK_α radiation was used.

When gathering temperature dependent WAXD spectra, an Anton Paar TTK450 temperature control cell was used.

WAXD analysis was carried out on a film of 1-mm thickness, prepared by compression molding with controlled cooling to 30°C/min, after aging for 21 days.

The application of the least-squares fit procedure elaborated by Hindeleh and Johnson[26] gave the degree of crystallinity by weight (C_{WAXD}).

Small Angle X-ray Scattering

The SAXS measurements were performed in a MBraun system by utilizing CuK_α radiation from a Philips PW1830 X-ray generator. The patterns were recorded by a position sensitive detector in the scattering angular range 0.1–5.0° 2θ and corrected for the blank scattering. A constant continuous background scattering[27] was subtracted and the obtained intensity values

$\tilde{I}(s)$ were smoothed, in the tail region, with the aid of the $s\tilde{I}(s)$ versus $1/s^2$ plot.[28] Then Vonk's desmearing procedure[29] was applied and the one-dimensional scattering function was obtained using the Lorentz correction: $I_1(s) = 4\pi s^2 I\ (s)$, where $I_1(s)$ is the one-dimensional scattering function and I(s) is the desmeared intensity function.

The sum of the average thicknesses of the crystalline and amorphous layers was determined as the Bragg identity period D of the function $I_1(s)$.

SAXS Data Analysis

The evaluation of the SAXS patterns according to some theoretical distribution models[30] was carried out referring to the Hosemann model,[31] which assumes the presence of lamellar stacks having an infinite side dimension. This assumption takes into account a monodimensional electron density change along the normal direction to the lamellae.

The fitting procedure[30] of the calculated one-dimensional scattering function with the experimental one allows to optimize the values of the thicknesses and distributions of the crystalline and amorphous layers, the long period and the crystallinity, along with their distribution, associated to lamellar stacks.

Nuclear Magnetic Resonance in the Solid State (SS NMR)

^{13}C SS NMR spectra were recorded at 100.62 MHz on a Bruker DPX 400 instrument, powder samples were spun at 10 kHz in 4 mm ZrO_2 rotor at 25°C.

For SS NMR analysis, the sample must be in the form of fine powder to fill the rotor in a homogeneous way, otherwise the inhomogeneities can cause imbalances during rotation that in the worst case cause the breakage of the probe. The pellets of the samples were then ground in a cryogenic Retsch CryoMill ball mill. In this instrument the grinding jar is continually cooled with liquid nitrogen from the integrated cooling system before and during the grinding process to maintain the temperature at −196°C.

^{13}C single pulse excitation (SPE) NMR spectra, which allow the quantitative acquisition of both the amorphous and crystalline components of the samples, were recorded with an acquisition time of 50 ms and a repetition time of 20 s. ^{13}C cross polarization magic angle spinning (CPMAS) NMR spectra, which enhance the acquisition of the crystalline component, were recorded with an acquisition time of 50 ms, a repetition time of 20 s and a contact time of 2.5 ms.

256 transients were acquired for both experiments and the methyl of form I was used as an internal reference at 12.8 ppm.

Transmission Electron Microscopy

TEM images were obtained using a FEI Tacna 10, operating at an acceleration voltage of 100 kV and with a resolution of 0.34 nm.

Using a cryogenic microtome (Leica EM UC7), a thin layer (100 nm) was sectioned from the compression molded film at −70°C. This instrument operates at a temperature lower than the glass transition temperature of the sample, so this allows to maintain the morphology of the sample and improving the cutting conditions.

Atomic Force Microscopy

AFM micrographs were recorded by tapping-mode AFM using a Multimode Nanoscope V (Bruker).

Films of 1-mm thickness were prepared by compression molding of the samples PBET8 and PBET8-A2, for each sample a sufficiently smooth surface was obtained by a cryogenic microtome (Leica EM UC7) at −70°C. The samples PBET8 and PBET8-A2 were analyzed at different aging times: immediately after compression molding ($t = 0$ h), after 8 h and 24 h.

Mechanical Properties and Cut & Stick

The specimens for the mechanical testing were kept for 72 h at room temperature and 2000 bar.

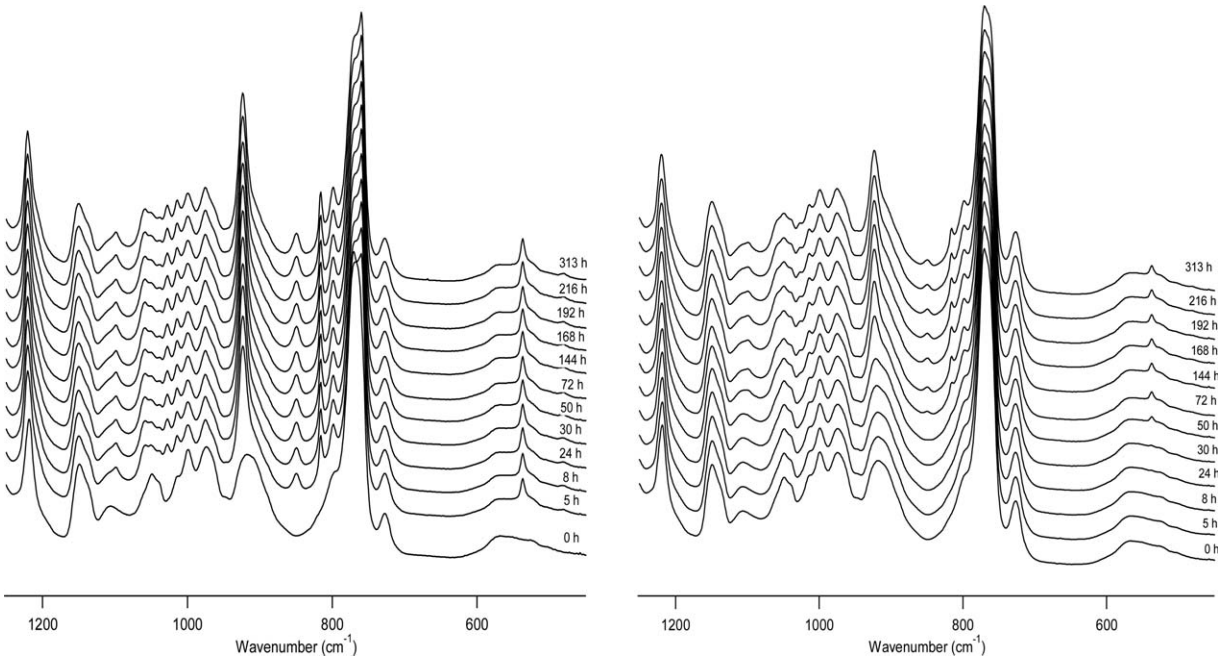

Figure 1. FTIR spectra of PBET5 (left) and PBET8 (right) as a function of the aging time.

The tensile properties of the samples (dimensions 75 mm × 12.5 mm × 2 mm) were measured using a Zwick Z030 at room temperature (ISO527).

The tension test was performed stretching the specimen (dimensions 50 mm × 2 mm × 2 mm) by 200% for 10 min (ISO 2285).

The compression test was performed at a temperature of 23°C for 22 h, with a compressive strain of 25%, the specimen used was a cylindrical disk of thickness 12.5 mm and a diameter of 29.0 mm (ASTM D395).

At least five measurements were performed for each sample.

The stress at break (MPa), elongation at break (%) tension set (%) and compression set (%) of the samples were measured with relative errors of max. 5%.

The hardness was measured on a Durometer Galileo A-200 according to ISO868.

The Cut & Stick test was carried out according to this method: a plate (dimensions 120 mm × 120 mm × 4 mm) was prepared by compression molding (ISO 8986-2) and then divided in 10 specimens (80 mm × 10 mm × 4 mm).

The specimens were left at room temperature for 10 days, and then cut in half with a scissors. After cutting (2 s) a pressure of 20 N was applied for 1 min on the cut sections, the samples are then allowed to stand for 3600 s. The subsequent tensile test allows to obtain the values of stress and elongation at break.

RESULTS AND DISCUSSION

The study by FTIR spectroscopy has been addressed to determine the different phases in the samples as reported in literature[32–37] and to calculate a crystallinity index to correlate with DSC, WAXD, and NMR results.

There are distinct differences in IR spectra of each sample from the time of molding ($t = 0$ h) and the complete transformation due to aging ($t = 313$ h) and among the samples after the aging period.

Figure 1 shows the registered spectra of PBET5 and PBET8 samples in the 450–1250 cm^{-1} range, where the most interesting bands are shown.

In the just molded samples (Supporting Information Figure S1) it is possible to see an absorption band at 918 cm^{-1}, characteristic of the amorphous phase[38] that shifts toward 923 cm^{-1} for the aged samples, it grows in intensity and its shape becomes narrower.

This new sharper band is attributable to form I (CH_2 and CH_3 rocking) and in particular to the crystalline phase of the copolymer samples, as well as for the bands at 1025, 1014, 849, 817, 798, and 538 cm^{-1} which are not present in the spectra of the just molded samples, but which appear and grow in intensity with increasing aging time.

Besides, the bands at 849 cm^{-1} (CH_2 and CH_3 rocking and CC symmetric vibration) and 817 cm^{-1} (CH_2 rocking) can be used to monitor the form transformation II → I[32].

The single peak at 725 cm^{-1} (Supporting Information Figure S1) confirms[39] the presence of random ethylene copolymerized with 1-butene because crystalline polyethylene would give a doublet at 720–730 cm^{-1}.

It is possible to distinguish[17] form I, twinned, and form I′, untwinned, from the bands at 810 and 792 cm^{-1} and at 1025 and 1008 cm^{-1} of a homopolymer sample, which have different intensity rates for the two forms, if A is the absorbance of a specific band, $A_{810} > A_{792}$ and $A_{1025} > A_{1008}$, is related to the presence of form I, in the opposite case there is form I′.

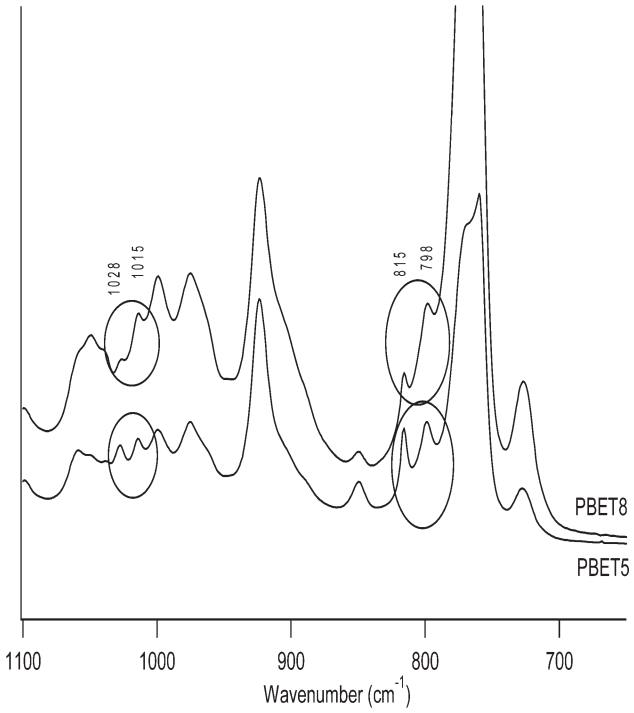

Figure 2. FTIR of PBET5 and PBET8 at aging time $t = 313$ h.

In the spectra of the studied copolymer samples, the corresponding bands are slightly displaced: for the samples PBET4 and PBET5 the bands at 815 and 798 cm^{-1} have about the same intensity as well as the bands at 1026 and 1013 cm^{-1} (Figure 2). It is possible to conclude that in these two samples both form I and form I′ coexist. For the samples PBET8, PBET8-A1 and PBET8-A2 the band at 798 cm^{-1} has a higher intensity than the band at 815 cm^{-1} and the band at 1014 cm^{-1} has a higher intensity than the band at 1025 cm^{-1} (Figure 2): this reveals the presence of the only form I′.

In addition, in PBET8-A1 and PBET-A2 spectra are present the characteristic bands of terPP at 1166, 898, and 840 cm^{-1}.

From the analysis of the bands attributable to the amorphous phase (918 cm^{-1}) and the crystalline (923 cm^{-1}) one, the crystallization kinetics of the samples was assessed.

To calculate the crystallinity index of the samples, the increase of the 923 cm^{-1} band compared with the 918 cm^{-1} one was evaluated, Rca was defined as the ratio between the intensity of the two bands calculated by curve fitting.

In Figure 3, the values of Rca, calculated for the samples as a function of aging time, are reported.

Samples PBET4 and PBET5 which contain respectively 4.1 and 5 wt % of C2 reach the plateau of the "Rca vs t" curve in a time shorter than the other samples, that is about 5 h instead of 24 h or 144 h.

It can be concluded that decreasing the C2 content in the copolymer there is an increase of both the crystallization rate and the index of crystallinity of the samples.

Besides it is confirmed the ability of terPP to speed up the crystallization process, Figure 3 shows that the curve referred to the sample PBET8, which has the same C2 content of samples PBET8-A1 and PBET8-A2, remains at zero till approximately 24 h and then reach the plateau at about 144 h, while as far as the other two samples are concerned, the plateau is already reached after 24 h.

It is also possible to distinguish forms I and I′ by DSC, because of the presence of melting endotherms at different temperatures[14,22], this feature has been used to confirm FTIR data regarding the type of crystalline form present in the studied samples.

Samples PBET4 and PBET5 with lower C2 content have two endotherms at ~38°C and ~52°C related to the melting of form I′ and I, while samples PBET8, PBET8-A1, and PBET8-A2 have a single melting peak at ~38°C characteristic of form I′.

Table II shows the data collected from the DSC analysis of the copolymer samples and of a homopolymer sample of poly-1-butene (HomoPB) by metallocenic catalysis, aged 10 days, together with the calculated[40] degree of crystallinity of the samples (C_{DSC}), which decreases with increasing C2 content, as well as the corresponding melting temperature.

The thermograms of the sample PBET5, which presents both forms I and I′, were registered at different aging times (Figure 4) to follow the development of the crystalline forms.

This shows that the sample PBET5 has two melting peaks at ~35°C and ~50°C, the first associated with the melting of the crystalline form I′ ($T_{mI'}$) and the second of form I (T_{mI}). The two endotherms grow together and the growth of one does not involve the decrease of the other, so the two forms coexist from the beginning till the end of the crystallization process. The melting enthalpy, calculated for the sum of the areas of the two endotherms, increases over time: the degree of crystallinity of the sample increases until it reaches a plateau in approximately

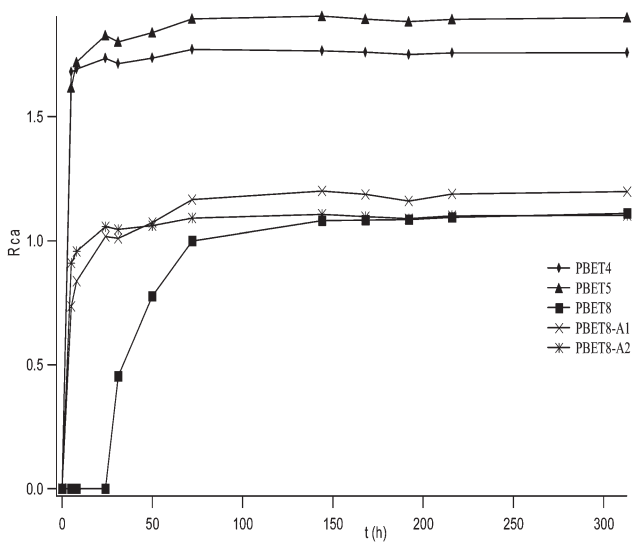

Figure 3. Ratio (Rca) between the intensity of the bands at 923 and 918 cm^{-1} as a function of aging time.

Table II. C2 Content, Melting Temperatures (T_{mI}, T_{mI}), Melting Enthalpy (ΔH_I, ΔH_I, $\Delta H_{I+\ I'}$) and Degree of Crystallinity (C_{DSC}) of the Examined Samples

		HomoPB	PBET4	PBET5	PBET8	PBET8-A1	PBET8-A2
C2	wt %	0	4.1	5	8	8	8.2
$Tm_{I'}$	°C		38.8	38.3	39.6	38.0	37.9
Tm_I	°C	116.3	54.6	51.7			
ΔH_I	J/g	47.7					
ΔH_r	J/g				11.11	10.37	8.46
ΔH_{I+r}	J/g		33.2	27.1			
C_{DSC}	%	38	27	22	9	8	7

one day of aging (Table III). Therefore the trend observed with FTIR analysis is confirmed.

WAXD analysis of polymer samples usually allows to determine the polymorphic form present in the material, in the case of forms I and I′ of poly-1-butene this is not possible because of the presence of the same crystalline structure.

However, the degree of crystallinity C_{WAXD} (Table I) was calculated from the spectra of the samples after aging, in fact, WAXD spectra of the samples just cooled from the melt show no crystalline peaks since the samples are in the amorphous state and crystallize only after aging (Figure 5).

The trend of the degree of crystallinity obtained from FTIR and DSC is also confirmed by WAXD data (Table I).

It was also carried out the measurement of the WAXD spectrum of PBET5 after aging at different temperatures (Supporting Information Figure S2): before the melting of the sample (25°C), during the melting (38°C) and after the melting of form I′ (42°C), during the melting (50°C) and after the melting (70°C) of form I.

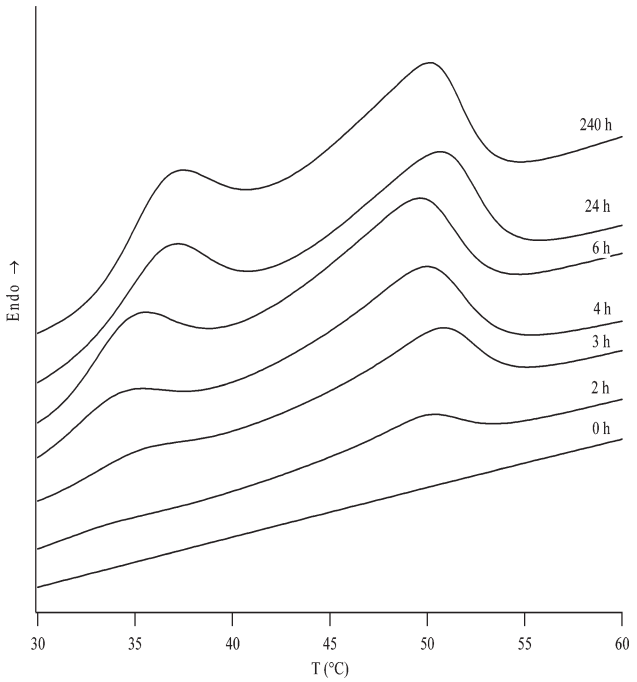

Figure 4. PBET5 thermograms at different aging times.

The intensity of the peaks decreases steadily with increasing temperature up to the complete melting of the sample, and it is not possible to see differences from when there are both forms and when, after the melting of form I′, only form I is left.

An effective analysis of the three-dimensional structure of the copolymer samples can be conducted by ^{13}C NMR in the solid state. The powder samples prepared with a cryogenic ball mill from pellets have been previously analyzed by ATR to ensure that the mill had not induced transformations or phase transitions in the material.

It was found that the milled powders of the aged samples PBET4 and PBET5 have an ATR spectrum similar to that of the film after aging and therefore the crystalline phase in both samples is present in both form I and I′, the same is the result for aged PBET8, PBET8-A1, and PBET8-A2 and therefore the crystalline phase is in form I′.

The ground powders of HomoPB and terPP were used as reference, the registered ATR spectra of HomoPB showed the only presence of form I.

^{13}C CPMAS NMR and ^{13}C SPE NMR spectra of the samples PBET4, PBET5, PBET8, PBET8-A1, PBET8-A2 and HomoPB and ^{13}C CPMAS NMR spectra of terPP were acquired.

It was made the assignment of the peaks relating to the 1-butene/ethylene copolymers[41] and to terPP in ^{13}C CPMAS NMR spectra of the samples (Figure 6).

Table III. DSC Data of PBET5 at Different Aging Time

t (h)	ΔH (J/g)	Tm_r (°C)	Tm_I (°C)	C_{DSC} (%)
0	0	0	0	0
2	5.7	34.1	49.8	5
3	11.0	35.4	50.4	9
4	19.0	34.6	49.7	15
6	21.6	35.1	49.3	17
24	24.2	36.8	50.4	19
240	25.9	37.1	49.9	21

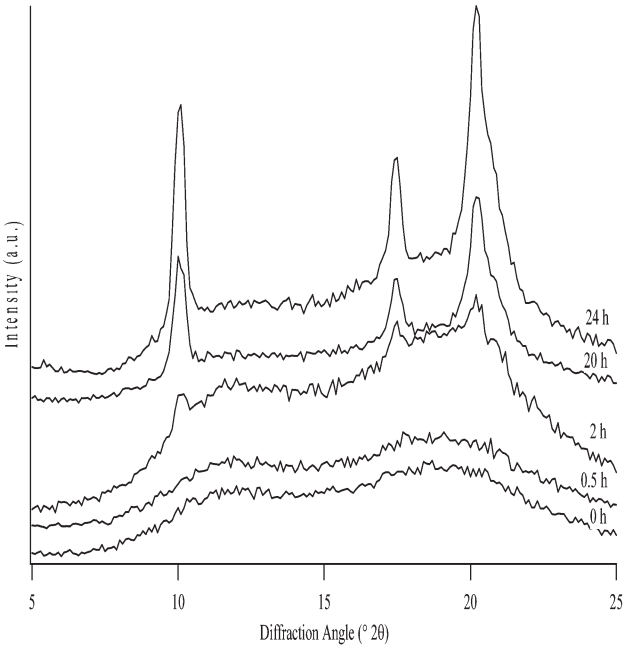

Figure 5. WAXD spectra of PBET5 at different aging time.

The copolymer samples have split signals at 11.8 and 12.8 ppm of methyl, at 26.0 and 27.0 ppm of methylene in the side chain, at 38.0 and 38.9 ppm of methylene on the main chain and at 32.2 ppm of methine.

It was not possible to assign all the signals of ^{13}C SPE NMR spectra, because in the range from about 22.0 to 44.0 ppm they do not appear resolved and distinguishable (Figure 6).

From literature[42] it was found that in the ^{13}C NMR SS spectrum of homopolymer of poly-1-butene the split of the peak relative to the methyl (at 11.8 and 12.8 ppm) is due to different forms of organization of the polymer chain. In particular the signal at 11.8 ppm is attributed to both amorphous phase and form II and the one at 12.8 ppm to form I. It is believed that form II and the amorphous phase have the same mobility and give a signal at the same chemical shift.

Referring to the results obtained by FTIR, DSC and WAXD, since it was not observed the presence of form II in the tested samples, the peak at 11.8 ppm was attributed exclusively to the amorphous phase.

As already done by FTIR, DSC and WAXD the evolution with aging time of form I/I′ by SS NMR was studied to determine if it is possible to distinguish the two forms by this technique.

The sample PBET5 was studied for this purpose. The milled powder was melted by placing the rotor with the sample between the plates of a press at 70°C.

^{13}C CPMAS NMR and ^{13}C SPE NMR were recorded after the melting at different aging times.

^{13}C CPMAS NMR spectra in Figure 7 shows the evolution of the spectra over time. At the initial time ($t = 0$ h) the intensity of the peak at 11.8 ppm is greater than that of the peak at 12.8 ppm, whereas after 24 h the ratio is reversed.

The same behavior is found in ^{13}C SPE NMR spectra.

Since the peak at 12.8 ppm is attributed to form I, it is confirmed that the sample crystallizes with aging time, and probably the same peak corresponds to form I′.

From ^{13}C SPE NMR spectra it was also possible to obtain the degree of crystallinity of aged samples, this calculation confirmed that the degree of crystallinity decreases with the ethylene content of the samples (Table IV).

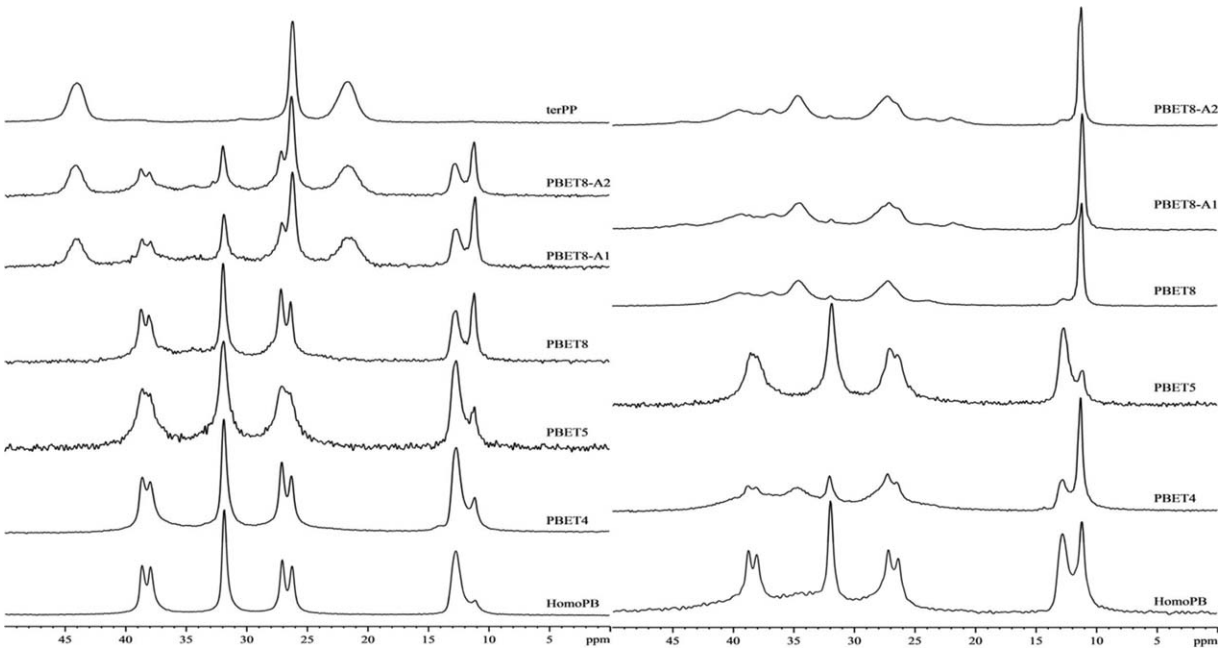

Figure 6. ^{13}C CPMAS NMR (left) and ^{13}C SPE NMR (right) spectra of the samples.

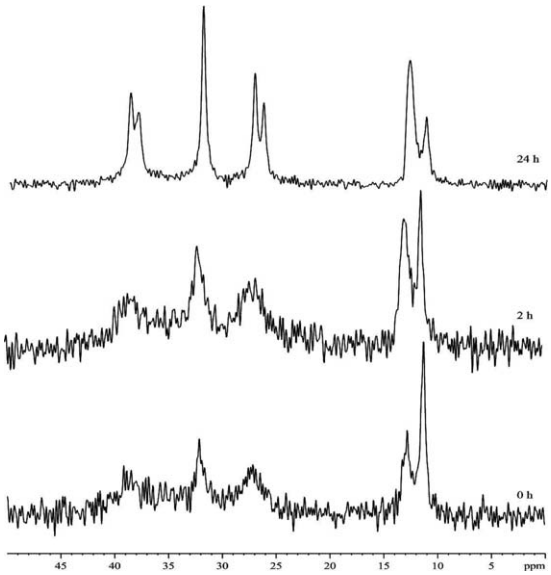

Figure 7. ^{13}C CPMAS NMR spectra of PBET5 at different aging time.

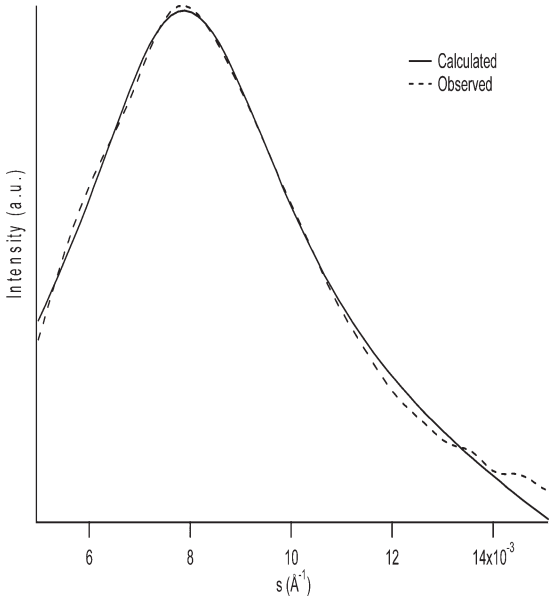

Figure 8. SAXS pattern (dotted line) of PBET5 and trace calculated by fitting procedure (solid line).

SAXS spectra were recorded with the purpose of studying the lamellar morphology and to compare the obtained results with TEM images.

The spectra of PBET4 and PBET8 show an extremely broad peak, therefore it is not possible to calculate the lamellar thickness distribution.

The spectra of the samples PBET8-A1 and PBET-A2 are similar in shape and two superimposed peaks are visible: also in this case the calculation of the lamellar thickness was not possible.

On the contrary the spectrum of the sample PBET5 (Figure 8) has allowed to determine the parameters, related to the lamellar morphology, shown in Table V.

Another technique that allows to obtain information about the lamellar morphology of the samples is TEM.

It was verified that the samples were morphologically homogeneous recording more images in different points of the film: Figure 9 shows the TEM image of sample PBET5 in which it is evident that the lamellar morphology is constituted by domains with small stacks of lamellae.

From Figure 9 the value of the long period (D) was calculated to see if the result corresponded to the one obtained from SAXS analysis.[43]

It was chosen an area in which the lamellae were well stacked and with an image processing program it was measured the gray scale along the red line in the upper right of Figure 9. Then a graph "grayscale vs. distance" was obtained (Supporting Information Figure S3).

Taking the ratio between the analyzed length and the number of "positive" peaks (contained in it) it was calculated the value of 10 nm corresponding to the long period, i.e., the average of the sum of the thicknesses of the crystalline and amorphous phases. This value corresponds quite well to the one obtained by SAXS analysis (Table IV).

Figure 10 shows the TEM image of PBET8, there are small domains of non-linear lamellae surrounded by a great amount of amorphous material, this is why SAXS analysis could not give the hoped results: the morphological order is too low.

Figure 11 shows the TEM image of PBET8-A2, before the addition in the production phase of terpolymer. The sample has few scattered, unorganized, and long lamellae, while it is observed that after the addition of the terpolymer (Figure 11), the lamellae are shorter and organize themselves in a homogeneous plot structure.

The same is true for PBET8-A2, but the morphology is less homogeneous.

AFM has proved very useful in accomplishing the morphological analysis, it was in fact possible to record images at different resolution (from 20 μm to 500 nm) of the same point of the sample to follow the lamellar growth and understand the role of terPP in the crystallization of the material.

For this purpose, the samples PBET8 and PBET8-A2 were analyzed at different aging time: immediately after the compression molding ($t = 0$ h), at 8 h and 24 h.

Table IV. Degree of Crystallinity of the Samples at Different C2 Content, Calculated From ^{13}C SPE NMR spectra

		HomoPB	PBET4	PBET5	PBET8	PBET8-A1	PBET8-A2
C2	wt %	0	4.1	5	8	8	8.2
C_{NMR}	%	46	30	24	9	6	7

Table V. Morphological Parameters of the Lamellar Stacks Obtained by SAXS Analysis of the PBET5 Sample: Long Period (D), Number of Lamellae (N), Thickness of the Crystalline (C), and Amorphous Layer (A), Along With Their Relative Distributions, ($\sigma_C/C = \sigma_A/A$, σ_D/D) and the Degree of Crystallinity by Volume (Φ_{SAXS})

A (nm)	*C* (nm)	*D* (nm)	*N*	Φc (%)	σ_D/D	σ_C/C	σ_A/A
7.2	3.1	10.3	4	30	0.38	0.48	0.48

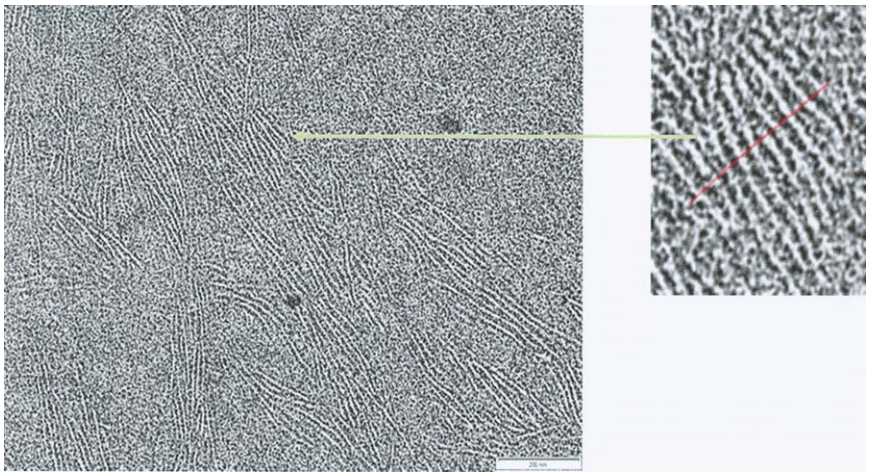

Figure 9. TEM image of PBET5. [Color figure can be viewed in the online issue, which is available at wileyonlinelibrary.com.]

Figures 12 and 13 show respectively AFM images of the sample PBET8 and PBET-A2 with a resolution of 2.5 μm at 0 h and 24 h: the areas in which is visible a lamellar growth are circled.

Thanks to an image analysis software, which allowed to process and refine the images obtained, the increase of the area filled by the lamellae was assessed from 0 h to 24 h. It was found out that the sample PBET8 (Figure 12) has an increase in the filled area of 2.28% while the sample PBET8-A2 (Figure 13) of 2.69%. It is observed that this increase is due to the growth of the lamellae and not to the formation of new nucleation centers, which are already present at time 0 h, besides there was an increase of the average length of the lamellae of about 53% for both samples.

PBET8 has longer lamellae (0.62 μm) than PBET8-A2 (0.20 μm) and comparing the images of the two samples (Figures 12 and 13) it is confirmed that they have a different morphology (as already seen from TEM images): the sample PBET8 has less nucleation centers but longer lamellae, the extent of lamellar growth is different because of the different type of nucleation.

Given the foregoing considerations, it is believed that the terPP present in PBET8-A2 is able to generate a greater number of nucleation centers, accelerating the crystallization process. The final value of crystallinity is not affected because even if the nucleation centers are more numerous, the lamellae grow less in length than those of the sample PBET8 and the value of the filled area remains similar.

The structural and morphological analysis performed by the various characterization techniques, allowed to determine the differences between the various copolymer samples which are evident with the change of C2 content and the introduction of terPP, it is therefore important to verify whether these differences are also reflected in a different mechanical behavior.

The values of elongation at break, tension set and compression set (Table VI) indicate that the elastic properties of the copolymers increase at the increasing of ethylene content, besides the hardness and the stress at break decrease.

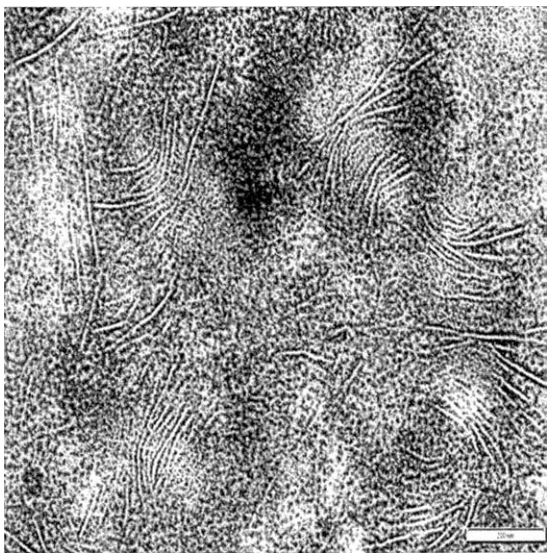

Figure 10. TEM image of PBET8.

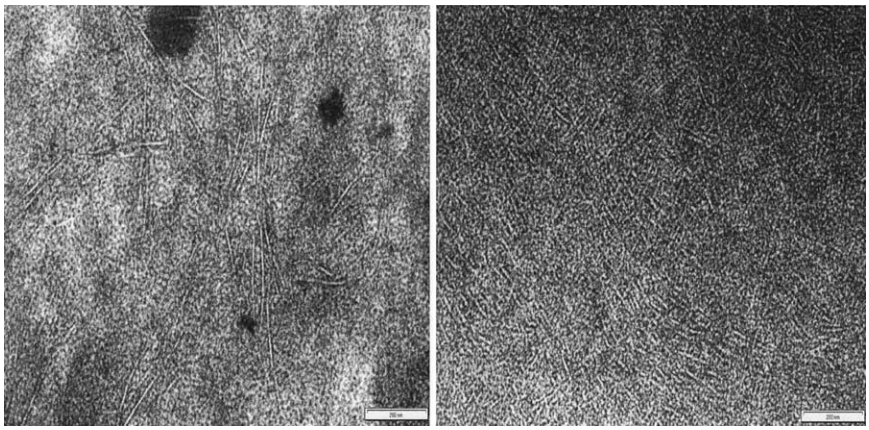

Figure 11. TEM image of PBET8-A1 before (left) and after (right) the addition of terPP.

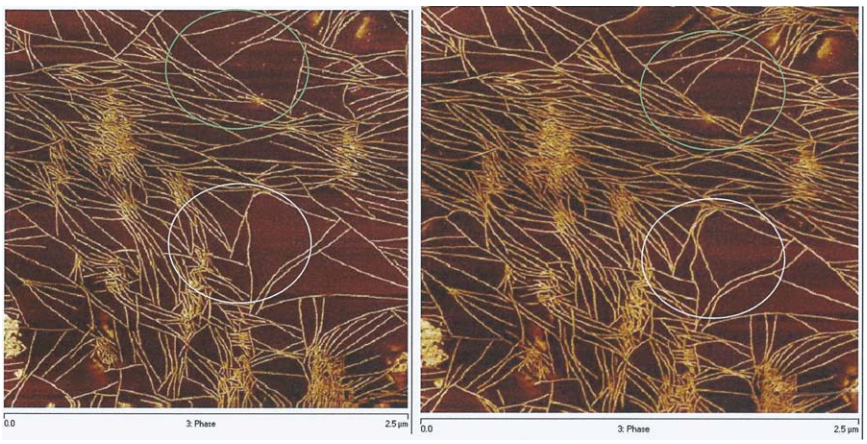

Figure 12. AFM images of PBET8 at aging time 0 h (left) and 24 h (right). [Color figure can be viewed in the online issue, which is available at wileyonlinelibrary.com.]

Thanks to the test Cut & Stick it was possible to evaluate the ability of self-welding of the studied materials. As a matter of fact one of the peculiar properties of these copolymers is the property of self-welding after being subjected to a cut without the use of glues. The phenomenon takes advantage of the low crystallinity of the samples and of the mobility of the polymer chains when subjected to mechanical stress such as a cut.

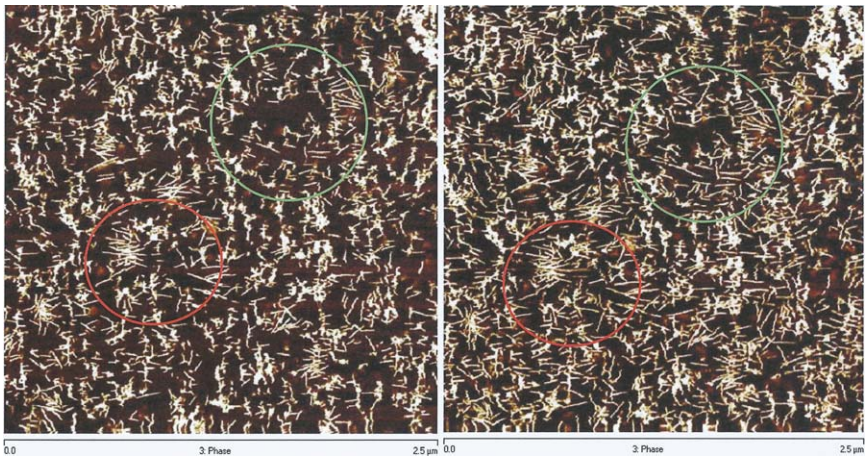

Figure 13. AFM images of PBET8-A2 at aging time 0 h (left) and 24 h (right). [Color figure can be viewed in the online issue, which is available at wileyonlinelibrary.com.]

Table VI. Mechanical Properties of the Copolymer Samples

		PBET4	PBET5	PBET8	PBET8-A1	PBET8-A2
Stress at break	MPa	24.4	20.5	2.6	14.8	6.4
Elongation at break	%	534	585	671	790	715
Hardness	Shore A	>90	>90	47	59	60
Tension set	%	76	60	41	9	15
Compression set	%	64	59	94	23	34

The samples tested were PBET4, PBET8, and PBET8-A1 because they are representative of three different structures: PBET4 and PBET8 do not contain terPP, the first presents both crystalline forms I and I′ and the second is completely in form I′, as well as the sample PBET8-A1 but it also contains terPP.

The results show that PBET4 has very low strength and elongation at break after cutting and welding, on the contrary PBET8 and PBET8-A1 have values of elongation at break very interesting. The average values of all tests are shown in Table VII.

The property of self-welding is connected to a high percentage of ethylene in the copolymer samples and to the presence of terPP. Indeed PBET8 and PBET8-A1 which contain 8% of C2 possess this property while PBET4 that contains only 4.1% is unable to self-welding.

The differences between the samples PBET8 and PBET8-A1 are attributed to the presence of terPP, which increases this feature even more in PBET8-A1.

By ATR technique it was possible to study the surface structure in the sections cut to observe any structural change immediately after cutting. This was possible because the ATR technique allows to obtain IR spectra of approximately the first 5 μm of the surface of the material.

A section was cut of each specimen whose surface was analyzed immediately after cutting and after different aging times to observe any changes.

ATR spectra of the samples show that with increasing aging time there is an increase of the crystallinity index of the samples. As in the FTIR study at different aging times, it was assessed the increase of crystallinity thanks to the Rca relationship between the intensity of the peak at 923 cm^{-1} and that of the peak at 918 cm^{-1}. (Supporting Information Figure S4).

After the cut, the crystallinity index of PBET8 and PBET-A1 is very similar and much lower than that of PBET4 as well as the increase with aging time (Supporting Information Figure S4), so it is assumed that the mobility of the polymer chains of samples PBET8-A1 and PBET8 is greater than that of the sample PBET4.

This, together with the Cut & Stick test results, allows to consider that the ability of self-welding of the surfaces just cut can be explained by the high mobility of the polymer chains, obtained by applying a stress that brings the sample in a state of lower crystallinity and allows their propagation between cut surfaces when they are in contact. The subsequent crystallization of the chains provides the resistance to breakage.

CONCLUSIONS

This study allowed to derive interesting conclusions on the structure, morphology and mechanical properties of this new class of 1-butene/ethylene random copolymers.

The samples cooled down from the melt are in the amorphous phase and crystallize in a mixture of form I and I′ or in pure form I′ with aging time, according to the C2 content, also the degree of crystallinity decreases and the crystallization proceeds slowly with increasing C2 content until it stabilizes after 24 h of aging or more.

It was highlighted that, at equal comonomer content, the presence of terPP accelerates the crystallization because it increases the nucleation centers while remaining unchanged the final degree of crystallinity, also it gives rise to a different lamellar morphology (shorter lamellae and less ordered organization).

The introduction of the comonomer produces an increase of the elasticity of the material and a decrease of the hardness, more evident with the increase of C2 content.

The presence, in the aged samples with higher C2 content, of the pure form I′ induces the ability to self-welding, even more accentuated by the presence of terPP. This is probably due to the fact that the stress applied at the time of cutting causes a partial melting, favored by the presence of form I′ that has a melting temperature lower than that of form I and so, due to the lower crystallinity in the section of the cut, is made easier the diffusion of polymer chains. This, together with the recrystallization that occurs with the increase of the aging time, promotes the enhance of strength at break of this material after self-welding.

The presence of terPP increases the mobility of the chains, because the area filled by the lamellae is greater in the samples that contain it, at equal C2 content, and the lamellae are shorter.

Table VII. Stress and Elongation At Break After Cut & Stick

		PBET4	PBET8	PBET8-A1
Stress at break	MPa	0.99	1.5	1.6
Elongation at break	%	10	220	260

This new class of materials combines high flexibility with good elasticity and ductility and can be processed directly or used as modifying agents in polymers.

REFERENCES

1. Natta, G.; Corradini, P.; Danusso, F.; Mantica, E.; Mazzanti, G.; Pino, P.; Moraglio, G. *J. Am. Chem. Soc.* **1955**, *77*, 1708.
2. Miller, R. L.; Holland, V. F. *Polym. Lett.* **1964**, *2*, 519.
3. Turner Jones A. *Polym. Lett.* **1963**, *1*, 455.
4. Natta, G.; Corradini, P.; Bassi, I. W. *Nuovo Cimento suppl.* **1960**, *15*, 52.
5. Aronne, A.; Napolitano, R.; Pirozzi, B. *Eur. Polym. J.* **1986**, *22*, 703.
6. Boor, J.; Youngman, E. A. *Polym. Lett.* **1964**, *2*, 903.
7. Zannetti, R.; Rossi Ferracini, E.; Celotti, G. *La Chimica e L'Industria* **1967**, *49*, 1060.
8. Cortazar, M.; Sarasola, C.; Guzman, G. M. *Eur. Polym. J.* **1982**, *18*, 439.
9. Hsu, C. C.; Geil, P. H. *J. Macromol. Sci. Phys.* **1986**, *B25*, 433.
10. Armeniades, C. D., Baer, E. *J. Macromol. Sci.* **1967**, *B1*, 309.
11. Nakafuku, C.; Miyaki, T. *Polymer* **1983**, *24*, 141.
12. Marigo, A.; Marega, C.; Cecchin, G.; Collina, G.; Ferrara, G. *Eur. Polym. J.* **2000**, *36*, 131.
13. Luciani, L.; Seppälä, J.; Löfgren, B. *Prog. Polym. Sci.***1988**,*13*,37.
14. Holland, V. F.; Miller, R. L. *J. Appl. Phys.* **1964**, *35*, 3241.
15. Geacintov, C.; Miles, R. B.; Schuurmans, H. J. L. *J. Polym. Sci. Part A-1: Polym. Chem.* **1966**, *4*, 431.
16. Chau, K.W.; Geil, P. H. *J. Macromol. Sci. Phys.* **1984**, *B23*,115.
17. Goldbach, G.; Peitscher, G. *Polym. Lett.* **1968**, *6*, 783.
18. Boor, J., Jr.; Youngman, E. A. *J. Polym. Sci. Part B: Polym. Phys.* **1964**, *2*, 903.
19. Azzurri, F.; Alfonso, G. C.; Gómez, M. A.; Martì, M. C.; Ellis, G.; Marco, C. *Macomolecules* **2004**, *37*, 3755.
20. Azzurri, F.; Gómez, M. A.; Alfonso, G. C.; Ellis, G.; Marco, C. *J. Macromol. Sci. Phys.* **2004**, *B43*, 177.
21. Marega, C.; Causin, V.; Marigo, A.; Saini, R.; Ferrara, G. *J. Nanosci. Nanotechnol.* **2010**, *10*, 3078.
22. De Rosa, C.; Auriemma, F.; de Ballesteros, O. R.; Esposito, F.; Laguzza, D.; Di Girolamo, R.; Resconi, L. *Macromolecules* **2009**, *42*, 8286.
23. Galimberti, M.; Martini, E.; Piemontesi, F.; Sartori, F.; Camurati, I.; Resconi, L.; Albizzati E. *Macromol. Symp.* **1995**, *89*, 259.
24. Resconi, L.; Camurati, I.; Malizia, F. *Macromol. Chem. Phys.*, **2006**, *207*, 2257.
25. De Rosa, C.; Auriemma, F.; Resconi, L. *Angew. Chem.* **2009**, *48*, 9871.
26. Hindele, A. M.; Johnson, D. J. *J. Phys. D: Appl. Phys.* **1971**, *4*, 259.
27. Vonk, C. G.; Pijpers, A. P. *J. Polym. Sci. Part B: Polym. Phys.* **1985**, *23*, 2517.
28. Vonk, C. G. *J. Appl. Crystallogr.* **1973**, *6*, 81.
29. Vonk, C. G. *J. Appl. Crystallogr.* **1971**, *4*, 340.
30. Marega, C.; Marigo, A.; Cingano, G.; Zannetti, R.; Paganetto, G. *Polymer* **1996**, *37*, 5549.
31. Hosemann, R.; Bagchi, S. N. Direct Analysis of Diffraction by Matter; North Holland: Amsterdam, **1962**.
32. Luongo, J. P.; Salovey, R. *J. Polym. Sci. Part B: Polym. Phys.* **1965**, *3*, 513.
33. Luongo, J. P.; Salovey, R. *J. Polym. Sci. Part A-2: Polym. Phys.* **1966**, *4*, 997.
34. Tadokoro, H.; Kitazawa, T.; Nozakura, S.; Murahashi, S. *Bull. Chem. Soc. Jpn.* **1961**, *34*, 1209.
35. Ukita, M. *Bull. Chem. Soc. Jpn.* **1966**, *39*, 742.
36. Lee, K. H.; Snively, C. M.; Givens, S.; Chase, D. B.; Rabolt, J. F. *Macromolecules* **2007**, *40*, 2590.
37. Sharma, P.; Tandon, P.; Gupta, V. D. *Eur. Polym. J.* **2000**, *36*, 2629.
38. Ruiz-Orta, C.; Alamo, R. G. *Polymer* **2012**, *53*, 810.
39. Tashiro, K. In Measurement of the Physical Characteristic of Polymers by Vibrational Spectroscopy; Everall, N. J.; Chalmers, J. M.; Griffiths, P. R., Eds.; Vibrational Spectroscopy of Polymer: Principles and Practice; John Wiley and Sons: Chichester, UK, **2007**, 143.
40. Jones, A. T. *J. Polym. Sci. Part B: Polym. Phys.*, **1963**, *1*, 455.
41. Belfiore, L. A.; Schilling, F. C.; Tonelli, A. E.; Lovinger, A. J.; Bovey, F. A. *Macromolecules*, **1984**, *17*, 2561.
42. Miyoshi, T.; Hayashi, S.; Imashiro, F.; Kaito, A. *Macromolecules* **2002**, *35*, 6060.
43. Causin, V.; Marega, C.; Marigo, A.; Ferrara, G. *Polymer* **2005**, *46*, 9533.